Author Manuscript

Author Manuscript

Author Manuscript

Author Manuscript

HHS Public Access

Author manuscript

Nat Chem Biol. Author manuscript; available in PMC 2014 July 01.

Published in final edited form as:

Nat Chem Biol. 2014 January ; 10(1): 76–84. doi:10.1038/nchembio.1389.

PITPs as Targets for Selectively Interfering With Phosphoinositide Signaling in Cells

Aaron H. Nile[1,2], **Ashutosh Tripathi**[1,3,*], **Peihua Yuan**[1], **Carl J. Mousley**[1], **Sundari Suresh**[4], **Iain Michael Wallace**[4], **Sweety D. Shah**[2], **Denise Teotico Pohlhaus**[3], **Brenda Temple**[5], **Corey Nislow**[6], **Guri Giaever**[6], **Alexander Tropsha**[3], **Ronald W. Davis**[4], **Robert P. St Onge**[4], and **Vytas A. Bankaitis**[1,2,*]

[1]Department of Molecular & Cellular Medicine, Department of Biochemistry & Biophysics, Department of Chemistry, Texas A&M University, College Station, Texas 77843-1114 USA

[2]Department of Cell & Developmental Biology, Lineberger Comprehensive Cancer Center, University of North Carolina School of Medicine, Chapel Hill, North Carolina 27599-7090 USA

[3]Laboratory for Molecular Modeling, Eshelman School of Pharmacy, University of North Carolina at Chapel Hill, Chapel Hill, North Carolina 27599-7355 USA

[4]Department of Biochemistry, Stanford Genome Technology Center, Stanford University, Palo Alto, CA 94304

[5]R. L. Juliano Structural Bioinformatics Core, University of North Carolina at Chapel Hill, Chapel Hill, North Carolina 27599-7260 USA

[6]Faculty of Pharmaceutical Sciences,, University of British Columbia, Vancouver, BC V6T 1Z3, Canada

Abstract

Sec14-like phosphatidylinositol transfer proteins (PITPs) integrate diverse territories of intracellular lipid metabolism with stimulated phosphatidylinositol-4-phosphate production, and are discriminating portals for interrogating phosphoinositide signaling. Yet, neither Sec14-like PITPs, nor PITPs in general, have been exploited as targets for chemical inhibition for such purposes. Herein, we validate the first small molecule inhibitors (SMIs) of the yeast PITP Sec14. These SMIs are nitrophenyl(4-(2-methoxyphenyl)piperazin-1-yl)methanones (NPPMs), and are effective inhibitors in vitro and in vivo. We further establish Sec14 is the sole essential NPPM target in yeast, that NPPMs exhibit exquisite targeting specificities for Sec14 (relative to related

Users may view, print, copy, download and text and data- mine the content in such documents, for the purposes of academic research, subject always to the full Conditions of use: http://www.nature.com/authors/editorial_policies/license.html#terms

*Co-corresponding authors: TEL: 979-862-3188, vytas@tamhsc.edu, tripathi@tamhsc.edu.

AUTHOR CONTRIBUTIONS

A.H.N was involved in all experimentation, design, data analysis, manuscript preparation, and figure production. A.T, with assistance from B.T. and D.T.P., designed computational experiments, data analysis, manuscript preparation, and figure production. P.Y. and C.J.M. performed electron microscopy, invertase and CPY experiments, and S.D.S generated site-directed mutants and purified proteins. I.W, C.N, S.S., R.P.S selected initial SAR compounds. performed and designed chemogenomic profiling. R.W.D. and G.G. advised chemogenomic studies. V.A.B was involved in all aspects of experimental design, data analysis, and manuscript preparation.

COMPETING FINANCIAL INTERESTS STATEMENT

The authors declare no financial conflicts.

Author Manuscript Author Manuscript Author Manuscript Author Manuscript

Sec14-like PITPs), propose a mechanism for how NPPMs exert their inhibitory effects, and demonstrate NPPMs exhibit exquisite pathway selectivity in inhibiting phosphoinositide signaling in cells. These data deliver proof-of-concept that PITP-directed SMIs offer new and generally applicable avenues for intervening with phosphoinositide signaling pathways with selectivities superior to those afforded by contemporary lipid kinase-directed strategies.

Lipid signaling modulates a wide range of cellular processes, including regulation of G-protein-coupled receptors and receptor tyrosine kinases at the plasma membrane[1], actin dynamics[2], transcription[3,4], and membrane trafficking[5]. A major pillar of eukaryotic lipid signaling is defined by phosphoinositides and the soluble inositol (Ins) phosphates derived from them[6,7]. Phosphatidylinositol (PtdIns) is an essential phospholipid that serves as metabolic precursor for both phosphoinositides and Ins-phosphates. While Ins-phosphates are chemically diverse, the phosphoinositide cabal is simpler. Yeast produce five phosphoinositides (PtdIns-3-phosphate, PtdIns-4-phosphate, PtdIns-5-phosphate, PtdIns-4,5-bisphosphate, and PtdIns-3,5-bisphosphate) while mammals produce seven; those synthesized by yeast as well as PtdIns-3,4-bisphosphate and PtdIns-3,4,5-trisphosphate[6]. This limited phosphoinositide cohort supports a diverse landscape of lipid signaling that modulates the actions of hundreds of proteins[7].

Specific inactivation of a target enzyme is a desirable instrument for dissecting mechanisms of lipid signaling in cells. This is especially true in the context of phosphoinositide signaling whose very diversification demands highly targeted approaches for clean analysis. However, specific genetic or chemical interventions at the level of individual lipid kinases, or compartment-specific interventions at the level of defined phosphoinositide species using Rapalog technologies[8,9], remain blunt experimental instruments. Such interventions exert pleiotropic effects because many effector activities are impaired upon inhibition of a target Ins-lipid kinase, or upon compartment-specific depletion of a specific phosphoinositide species.

PtdIns-transfer proteins (PITPs) of the Sec14 protein superfamily are key regulators of phosphoinositide signaling that specify discrete biological outcomes of PtdIns kinase action[10,11]. Deficiencies in individual Sec14-like PITPs compromise trafficking through the trans-Golgi network (TGN) and endosomal systems[12], phosphatidylserine decarboxylation to phosphatidylethanolamine[13], fatty acid metabolism[14], polarized growth[15], and fungal dimorphism[16]. Mutations in PITPs, or PITP-like proteins, are also root causes of mammalian neurodegenerative and lipid homeostatic diseases[17,18].

Various lines of evidence recommend PITPs as highly discriminating portals for interrogating phosphoinositide signaling, and identify PITPs as unexploited avenues for chemical inhibition of select phosphoinositide signaling pathways in cells. Herein, we exploit the yeast system to make the case. We validate the first chemical inhibitors of a PITP, demonstrate an exquisite in vivo specificity of action for such compounds, and propose a chemical mechanism for how these SMIs exert their inhibitory effects. These studies deliver proof-of-concept that PITP-directed approaches afford powerful advantages for chemically intervening with phosphoinositide signaling, and that the selectivities

Author Manuscript Author Manuscript Author Manuscript Author Manuscript

achieved are superior to those delivered by strategies targeting individual PtdIns-kinase isoforms or individual phosphoinositide species.

RESULTS

Candidate Sec14-directed SMIs

Sec14, the major yeast PITP, is an essential protein required for membrane trafficking through the TGN/endosomal system[12]. Chemogenomic profiling of 188 inhibitors of yeast growth identified a candidate for a Sec14-directed SMI[19]. This compound, 4130-1278 (**1**), is a 4-chloro-3-nitrophenyl)(4-(2-methoxyphenyl) piperazin-1-yl)methanone (NPPM). Since 4130-1278 exhibited mediocre potencies, and limited water solubility, we evaluated 13 other NPPM-like SMIs as Sec14 candidate inhibitors (Supplementary Results, Supplementary Fig. 1a). One such derivative, 4130-1276 (**2**), showed superior water solubility and arrested growth of a *sec14*Δ/*SEC14* heterozygous strain at 10-fold lower concentrations than those observed for 4130-1278 (Supplementary Fig. 1b).

Chemogenomic profiling of ca. 6200 yeast deletion strains correlated gene-dosage with yeast sensitivity to 4130-1278 or 4130-1276 challenge on a genome-wide scale (Supplementary Fig. 2a–f). The profiling identified *sec14*Δ/*SEC14* heterozygous diploid cells as the most sensitive to 4130-1278 and 4130-1276 challenge of all homozygous Δ/Δ and heterozygous Δ/+ diploids tested (non-essential and essential gene queries, respectively; Supplementary Fig. 2a–f). A limited set of other genes was also identified for which dosage reduction decreased fitness in the presence of 4130-1278 and 4130-1276 (Supplementary Fig. 2c, f). Gene functions identified in the more extensive 4130-1276 hit list included Golgi trafficking, sporulation, exocytosis, vacuolar transport, and lipid metabolism. A number of high scoring chemogenomic interactions, include phospholipase D (*SPO14*), a strong synthetic interactor with *sec14-1*^{ts} [10,20] and the phospholipase D regulator *SRF1*[21], were independently recognized in genome-scale synthetic genetic array (SGA) screens that employed *sec14-1*^{ts} as query allele[22,23].

Expansion of the candidate Sec14-directed SMI set

In focused searches for additional candidate Sec14-targeted SMIs, an expanded set of 34 compounds was assembled around the 4130-1276 scaffold. For initial rounds of compound selection, the Chembridge library was filtered using Similarity Search (Marvin Applet tool, Hit2Lead – Cambridge database). The filter clamped structural similarity to ca. 80% of the query 4130-1276 molecule and highlighted functional groups as sites for diversification (Supplementary Fig. 3a, b). NPPMs 4130-1276, 67170-49 (**3**) and 6748-481 (**4**) were chosen for study because these were potent growth inhibitors. The closely related 5564-701 (**5**) elicited no growth inhibitory effects and served as negative control. Structures of the five NPPMs of interest are shown in Figure 1a.

Sensitivity to NPPM is a function of Sec14 levels

Dose response experiments showed NPPM sensitivity was related to cellular Sec14 levels. NPPM 6748-481 served as representative SMI in these assays as it was the most water soluble bioactive compound and the most potent growth inhibitor. The half-maximal

Author Manuscript Author Manuscript Author Manuscript Author Manuscript

inhibitory concentration (IC_{50}) for 6748-481 was 2.9 ± 0.6 μM for WT haploid cells (Fig. 1b). When endogenous Sec14 levels were reduced ~7-fold by driving *SEC14* expression from a truncated promoter (*SEC14*$^{P\text{-}136}$) [24], the IC_{50} fell proportionately. The effect was specific as *SEC14*$^{P\text{-}136}$ haploids were not sensitized to the inactive 5564-701 (Fig. 1b), and elevated Sec14 levels enhanced resistance to 6748-481 (Fig. 1c).

NPPMs inhibit Sec14 in vitro

As Sec14 is not an enzyme, its activity is operationally defined by exchange of PtdIns and PtdCho between membranes in vitro[10]. NPPMs 67170-49, 6748-481 and 4130-1276 displayed potent and dose-dependent inhibitions of Sec14-catalyzed [^{3}H]-PtdIns transfer in a purified system. The IC_{50}s ranged from 175–283nM (Fig. 1d). At these concentrations, the Sec14:NPPM molar stoichiometries were ca. 1:1.

Two results excluded trivial possibilities that NPPMs interfered with Sec14 activities via non-specific membrane-active effects. First, biologically inactive NPPMs (5564-701) failed to diminish Sec14-catalyzed PtdIns-transfer at concentrations 500-fold above the IC_{50}s measured for Sec14-active NPPMs (Fig. 1d; Supplementary Fig. 4). Second, neither of the Sec14-active NPPMs tested (6748-481 and 4130-1276; 40μM) interfered with [^{3}H]-PtdIns transfer activities of other yeast Sec14-like PITPs (Sfh1–Sfh5[25]) -- even at concentrations ~200-fold greater than the corresponding Sec14 IC_{50}s (Fig. 1e). Sfh protein indifference to NPPMs demonstrated selectivity of the SMIs for Sec14 as Sfh PITPs share 23%–64% primary sequence identity with Sec14 (43%–89% similarity). That Sfh1-mediated transfer activities were not inhibited underscored the Sec14 selectivity of these NPPMs as Sfh1 is the closest known Sec14 homolog[26].

NPPM structure activity relationships

Forty-six NPPM-like molecules were evaluated for structure-activity relationships (SAR) for Sec14 inhibition. The cumulative SAR data assigned the relative importance of each NPPM functional group to activity as Sec14 inhibitor (IC_{50}<10μM in vitro activity threshold). SAR reported an obligatory requirement for *ortho*-Cl in the Cl-nitrophenyl (i.e. activated aryl halide) NPPM moiety (Fig. 2a; Supplementary Figs. 3,4). Either Cl- removal (4130-1276 vs. 5355-152 [**6**]), or Cl- shift to the *para* position (4130-1276 vs. 5658-722 [**7**]), increased the Sec14 IC_{50} >500-fold (Fig. 2b). The linker ketone that connects the Cl-nitrophenyl and piperazinyl groups was key. Its modification reduced NPPM potency in vitro by 30-fold (6748-481 vs. 5263-433 [**8**]). The NO_2-group also contributed to NPPM potency. Its removal resulted in a ~10-fold increase in IC_{50} (6748-481 vs. 5357-399 [**9**]; Supplementary Fig. 4). Addition of hydrophobic functional groups to the NPPM fluorobenzene tail enhanced potency ca. 4-fold (compare 5348-909 [**10**] with 6748-481, 7276-196, [**11**] and 6828-980 [**12**]). However, extending the linker that bridges the piperazinyl and fluorobenzene groups by a single carbon reduced NPPM potency (5348-909 vs. 5356-684 [**13**]; Supplementary Figs. 3,4).

Sec14 inhibition and the NPPM halide

The *ortho*-Cl requirement on the activated aryl halide raised the question of how halide identity influences NPPM potency. A variable aryl halide series was assembled

Author Manuscript Author Manuscript Author Manuscript Author Manuscript

[(BBV34896-755 [**14**], BBV34846-244 [**15**], Z1082669-326 [**16**]), and 6748-481 was resynthesized for inclusion in the series (BBV34846-247 [**17**]). The Cl-, Br- and I-derivatives (4130-1276 and 6748-481; BBV34846-244; Z1082669-326) exhibited potencies superior to those of the H-, CH_3- or F-derivatives (5355-152, 5348-723 [**18**], BBV34896-755). In rank order: Br-NPPM > I-NPPM ≥ Cl-NPPM (6748-481; BBV34846-247) ≫ F-NPPM, CH_3-NPPM, H-NPPM (Fig. 2c, Supplementary Fig. 4). Consistent with in vitro data, Cl-, Br- and I- versions were potent growth inhibitors, whereas H-, CH_3- and F- derivatives were not (Supplementary Fig. 3).

Six 'NO_2-less' derivatives, differing in halide chemistry and/or position, were evaluated (5356-628 [**19**], 5356-350 [**20**], 5567-782 [**21**], 5357-399, 5353-036 [**22**], 7329-906 [**23**], 5355-139 [**24**], 5528-054 [**25**]). The relative potencies of these compounds as Sec14 inhibitors were also directly proportional to the atomic mass and lipophilicities of the *ortho*-halide, and inversely proportional to halide electronegativity (Fig. 2d, Supplementary Fig. 4). The *ortho*-halide requirement for SMI activity was conserved (Fig. 2e, Supplementary Fig. 4). Parallel in vivo experiments demonstrated Cl-, Br- and I- compounds potently inhibited growth, whereas H-, CH_3- and F- derivatives did not (Supplementary Fig. 3).

NPPM binding models

NPPMs are amphipathic molecules that partition into apolar environments ($C_{log}P \sim 3.0$), suggesting NPPMs load into the Sec14 hydrophobic pocket during phospholipid exchange. To address how Sec14 binds NPPMs, a 1400Å^2 virtual pocket surface was modeled to form a boundary for unconstrained docking routines using 6748-481 as ligand (Supplementary Fig. 5). Multiple independent simulations, using several docking platforms, produced >3000 binding solutions that reduced themselves into 6 representative modes. These modes shared certain features with regard to Sec14::6748-481 interactions, but exhibited unique features as well (Supplementary Figs. 6,7). Two pose classes (modes 1,2 and modes 3,4) represented mirror images where orientations of bound 6748-481 were rotated 180° around the NPPM long axis. Another pose class (modes 5,6) shifted the 6748-481 binding site down the hydrophobic pocket. Sec14::NPPM interaction fingerprints highlighted how modes 5,6 forced NPPM polar groups into hydrophobic environments (Supplementary Figs. 6,7). This unappealing feature led us to reject mode 5,6 poses from consideration.

Fingerprints common to modes 1,2 and 3,4 included intercalation (in flipped orientation) of the 6748-481 fluorobenzene tail into the narrow hydrophobic cleft lined by Sec14 residues L_{232}, F_{228}, F_{225}, I_{240}, F_{221}, L_{179}, I_{214}, and M_{177} (Supplementary Figs. 6,7), and wedge of the fluoro-benzyl moiety between the side chains of F_{228} on one side and F_{212} and M_{177} on the other; thereby consolidating a network of hydrophobic and π-π stacking interactions. A second common fingerprint inter-digitated the 6748-481 chloro-nitrophenyl group in a hydrophilic subdomain of the Sec14 pocket where it set within H-bonding distance (1.5–3.5Å) to residues framing the Sec14 PtdCho headgroup-coordinating substructure (S_{173}, Y_{111}, Y_{122}, Y_{151}; Supplementary Figs. 6,7). All modes predicted NPPM-binding was sterically incompatible with PtdIns/PtdCho-binding (Supplementary Fig. 7b).

Modes 1,2 were distinguished from modes 3,4 by orientation of the 6748-481 ketone. Modes 1,2 anchored the ketone via H-bond interactions with S_{201}, whereas modes 3,4 assigned

Author Manuscript Author Manuscript Author Manuscript Author Manuscript

ketone interactions with Y_{151}. Modes 1 and 2 were further distinguished by their mirror-image orientation of the activated aryl halide. Mode 1 anchored the nitro- group by interactions with residues S_{173}/Y_{122} and the halide with Y_{111}/S_{173}. Mode 2 featured nitro- and halide interactions with S_{173} and Y_{111}/Y_{122}, respectively. Mode 3 assigned interactions of the nitro- and halide groups with residues S_{173} and Y_{111}, respectively, whereas mode 4 projected both the nitro- and halide groups engage S_{173}/Y_{111}. In sum, the solution sets projected Sec14 S_{173}, Y_{111}, Y_{122}, and Y_{151} interactions with activated aryl halide (albeit in flipped orientations), and anchor of the ketone to S_{201} or Y_{151}.

NPPM-resistant Sec14

The NPPM docking models made distinguishing predictions regarding which missense substitutions should diminish NPPM binding without affecting Sec14 activity. The corresponding Sec14 proteins were purified and assayed for PtdIns transfer activity. Residue S_{173} was of particular interest as it was consistently identified as highest scoring NPPM-interacting residue in docking simulations. Indeed, S_{173}C rendered Sec14 resistant to inhibition by NPPM 6748-481 in vitro -- even at concentrations approaching NPPM solubility limits (>736-fold more resistant than Sec14: Supplemental Figs. 8a). Specificity of effect was evident by the more modest NPPM-resistance exhibited by Sec14^{T175C}(Supplemental Figs. 8a), and Sec14^{S173C} resistance translated across the spectrum of Sec14-active NPPMs (Supplementary Fig. 8b, c). Strong reductions in 6748-481 sensitivity were also scored for Sec14^{Y111A}, Sec14^{Y151A} and Sec14^{S201C} (Fig. 3a, Supplemental Fig. 9a–c). The corresponding PtdIns-transfer activities were 337-, 140- and 22-fold less sensitive to 6748-481 inhibition (Fig. 3a, Supplemental Fig. 9a–c). Sec14^{Y111F}, Sec14^{Y122A}, Sec14^{M177C} and Sec14^{Y122F} showed only ~2- to 5-fold reductions in the same (Fig. 3a, Supplemental Fig. 9a, b, d, e.), whereas Sec14^{Y151F} displayed modestly enhanced sensitivity to 6748-481 (Fig. 3a, Supplemental Fig. 9a, b, e).

Sec14 is the sole essential NPPM target

Two lines of evidence demonstrated that Sec14 represents the sole essential NPPM target in cells. First, yeast expressing Sec14^{S173C} were resistant to challenge with 6748-481 (Fig. 3b). The second came from exploitation of ‘bypass Sec14’ mutants that no longer require Sec14 for viability. Genetic inactivation of the CDP-choline pathway for PtdCho biosynthesis (*cki1*Δ), or of the oxysterol binding protein homolog Kes1 (*kes1*Δ), effects ‘bypass Sec14’[27–30]. Both *cki1*Δ and *kes1*Δ cells were indifferent to 6748-481, 67170-49 or 4130-1276 (Fig. 3c).

NPPM challenge phenocopies genetic inactivation of Sec14

Sec14 promotes membrane trafficking through the TGN/endosomal system by coordinating PtdCho and PtdIns-4-phosphate (PtdIns-4-P) metabolism[22,28,30]. Thermal inactivation of Sec14 (by shift of *sec14-1*^{ts} mutants to 37°C) provoked intracellular accumulation of cargo-engorged TGN/endosomes. These morphological phenotypes were recapitulated in WT and *SEC14*$^{P-136}$ cells intoxicated with NPPMs 6748-481, 67170-49 or 4130-1276 (Supplementary Fig. 10). Mock challenge with DMSO, or with inactive 5564-701 control, had no effect. The *kes1*Δ and *cki1*Δ ‘bypass Sec14’ mutants were unaffected by 6748-481,

Author Manuscript Author Manuscript Author Manuscript Author Manuscript

67170-49, or 4130-1276 (Supplementary Fig. 11), and cells expressing Sec14^{S173C} were similarly unperturbed by NPPM challenge (Supplementary Fig. 12).

The trafficking defects induced by NPPM-poisoning were also on display when transport and/or recycling of cargo through the TGN/endosomal system were analyzed. Endocytic transport of the bulk membrane tracer FM4-64 to the limiting vacuole membrane (Supplementary Fig. 13a, b), and recycling of endocytosed Snc1 v-SNARE from TGN/endosomes to the cell surface, were both retarded by 6748-481, 67170-49 or 4130-1276 (Supplementary Fig. 14a, b). Mock challenge with DMSO or 5564-701 was without effect. Trafficking of secretory invertase to the cell surface was also impaired upon 6748-481, 67170-49, or 4130-1276 challenge, but not by 5564-701 or DMSO (Supplementary Fig. 15). NPPM-induced FM4-64, GFP-Snc1, and invertase trafficking defects were corrected by *kes1*Δ (Supplementary Figs. 16a–d). Sec14^{S173C} expression similarly rendered invertase secretion resistant to inhibition by Sec14-active NPPMs, (Supplementary Fig. 17).

The effects of NPPM challenge on transit of vacuolar carboxypeptidase Y (CPY) through the TGN/endosomal system were monitored by pulse-chase radiolabeling. Impaired trafficking from ER or TGN compartments was diagnosed by accumulation of CPY precursor forms (p1 and p2)[31]. Pools of p1CPY, and particularly of p2CPY, accumulated when *sec14-1*^{ts} yeast were shifted to restrictive temperatures (37°C) and upon treatment of WT or *SEC14*$^{P\text{-}136}$ cells with NPPMs 6748-481, 67170-49 or 4130-1276 (Supplementary Fig. 18a, b). Neither DMSO, nor 5564-701, impaired CPY transport from ER or TGN/endosomal compartments in WT or *SEC14*$^{P\text{-}136}$ cells. The inhibitory effects of Sec14-active NPPMs on CPY trafficking were dose-and time-dependent (Supplementary Fig. 19a, b), and were poorly reversible. Precursor CPY forms failed to chase to mCPY – even after a 2hr washout period with cycloheximide (Supplementary Fig. 20). Finally, NPPM 6748-481, 67170-49, and 4130-1276-mediated inhibition of CPY transit through the secretory pathway was remediated in *kes1*Δ and *cki1*Δ 'bypass Sec14' mutants (Supplementary Fig. 21, a, b), and in cells expressing Sec14^{S173C} as sole Sec14 source (Supplementary Fig. 21c).

NPPMs discriminate between phosphoinositide pools

Sec14 potentiates activities of both essential yeast PtdIns 4-OH kinases in vivo (i.e. Stt4 and Pik1)[10,32–34]. We therefore tested whether bulk PtdIns-4-P production was sensitive to inhibition by Sec14-active NPPMs. In these experiments, *sac1* mutants inactivated for the major yeast PtdIns-4-P phosphatase were employed because these mutants accumulate PtdIns-4-P to high levels[33,35]. This accumulation simplifies PtdIns-4-P biosynthetic rate measurements, and increases statistical power of PtdIns-4-P quantification. Challenge with 6748-481, 67170-49, 4130-1276, reduced bulk PtdIns-4-P levels by ~40% compared to levels recorded when cells were challenged with DMSO or 5564-701 (Supplementary Fig. 22a). Neither challenge with 6748-481, nor with 5564-701, affected PtdIns-3-P or PtdIns-4,5-bisphosphate (PtdIns-4,5-P_2) levels when compared to vehicle alone (Supplementary Fig. 22b, c).

NPPM selectivity on phosphoinositide homeostasis in WT yeast was also on display in vital imaging assays using isomer-selective biosensors. To probe status of PtdIns-4,5-P_2 pools, we monitored intracellular distribution of the GFP-2xPH$^{PLC\delta1}$ PtdIns-4,5-P_2 biosensor. This

Author Manuscript Author Manuscript Author Manuscript Author Manuscript

reporter localized to the plasma membrane in a PtdIns-4,5-P_2-dependent manner -- as evidenced by biosensor release into the cytoplasm upon inactivation of a temperature-sensitive version of the single yeast PtdIns-4-P 5-OH kinase (Mss4; Supplementary Fig. 22d, e). In accord with [^{3}H]-inositol radiolabeling data, GFP-2xPH$^{PLC\delta1}$ remained bound to plasma membrane after 3h incubation of cells with Sec14-active SMIs. Release of GFP-2xPH$^{PLC\delta1}$ from plasma membrane was not observed upon inactivation of other PtdIns kinases (Supplementary Fig. 22d, e).

Status of TGN/endosomal PtdIns-4-P pools was queried using two biosensors; GFP-GOLPH3 and GFP-2xPH$^{Osh2\ 36–38}$. Optimal association of both reporters with TGN/endosomal compartments was unaffected in cells devoid of PtdIns-3-phosphate and PtdIns-3,5-P_2 (*vps34*Δ), but was Pik1-dependent as evidenced by release from these organelles upon shift of *pik1*^{ts} mutants to 37°C (Supplementary Fig. 23a–d). Thermal inactivation of Sec14 (*sec14*^{ts} mutant, 37°C condition), or intoxication of yeast with 6748-481, 67170-49, or 4130-1276, similarly released GFP-2xPH^{Osh2} from TGN/endosomal structures (Fig. 4a, b). A compartmental pool-specificity was evident for NPPM-mediated interference of PtdIns-4-P signaling in these experiments. In addition to the Sec14- and Pik1-dependent TGN/endosomal PtdIns-4-P pool, GFP-2xPH^{Osh2} registered an Stt4-dependent plasma membrane pool of this phosphoinositide (Fig. 4a, b; Supplementary Fig. 23a, b). Challenge of WT cells with 6748-481, 67170-49 or 4130-1276 (but not 5564-701 or DMSO) released GFP-2xPH^{Osh2} from TGN/endosomal compartments -- without compromising biosensor targeting to the plasma membrane (Fig. 4a, b). In that regard, we previously showed that *kes1*Δ rescues growth defects of *pik1*^{ts}, but not *stt4*^{ts}, mutants at semi-permissive temperatures[29] – identifying Kes1 as an antagonist of Pik1-dependent PtdIns-4-P signaling. The *kes1*Δ ‘bypass Sec14’ mutant retained GFP-2xPH^{Osh2} on TGN/endosomal membranes in the presence of 6748-481, 67170-49, or 4130-1276 (Supplementary Fig. 24a, b).

Compartmental pool-specificities for NPPM-mediated interference of PtdIns-4-P signaling were also evident in GFP-GOLPH3 imaging experiments. The effects of genetic and NPPM-mediated Sec14 inactivation on GFP-GOLPH3 localization differed from those observed for GFP-2xPH^{Osh2} as these conditions effected morphological derangement of GFP-GOLPH3-positive TGN/endosomal compartments. Significant, but more limited, release of the reporter from TGN/endosomal membranes was observed (Fig. 4c, d; Supplementary Fig. 23c, d).

NPPMs discriminate between local PtdIns-4-P pathways

The GFP-2xPH^{Osh2} imaging results demonstrated Sec14-active SMIs disrupted PtdIns-4-P signaling in a compartment-specific manner (TGN/endosomes vs. plasma membrane). The distinct biological activities of Sec14 and the Sec14-like Sfh4 provided a more discerning test of whether Sec14-active NPPMs distinguished between parallel PtdIns-4-P signaling pathways that operate in the same endomembrane system. Sec14 and Sfh4 both control PtdIns-4-P production in TGN/endosomes. Unlike Sec14, Sfh4-dependent PtdIns-4-P signaling supports phosphatidylserine (PtdSer) decarboxylation to phosphatidylethanolamine (PtdEtn) in those compartments (Fig. 5a) [13]. As PtdEtn is an

Author Manuscript Author Manuscript Author Manuscript Author Manuscript

essential lipid, loss of Sfh4 activity resulted in Etn auxotrophy when the PtdSer decarboxylase 1 pathway was incapacitated (*psd1*Δ; Fig. 5b).

Because Sfh4 was not inhibited in vitro by Sec14-active NPPMs, we examined whether Sec14-active SMIs respected the PtdIns-4-P pool-selectivities of these distinct PITP-dependent metabolic circuits. Thus, *psd1*Δ yeast were reconstituted for $Sec14^{S173C}$ expression (to circumvent NPPM-induced growth defects associated with Sec14 inactivation), and cells were intoxicated with 6748-481. NPPM challenge failed to impose Etn auxotrophy onto the *PSD1* control, or onto the isogenic *psd1*Δ derivative (Fig. 5b) – thereby demonstrating that Sfh4 retained biological activity in the face of Sec14-active NPPM.

These phenotypic results were confirmed by [^{3}H]-serine radiolabeling experiments that measured Sfh4-dependent decarboxylation of PtdSer to PtdEtn in TGN/endosomes. NPPM 6748-481 challenge of *psd1*Δ mutants did not compromise PtdSer decarboxylation in vivo. This result was observed regardless of whether *psd1*Δ mutants expressed Sec14 (TGN/endosomal trafficking was blocked) or $Sec14^{S173C}$ (cells remained competent for TGN/endosomal trafficking; Fig. 5c). Thus, NPPM challenge failed to interfere with Sfh4-dependent PtdIns-4-P signaling in TGN/endosomes even as it strongly impaired Sec14-dependent PtdIns-4-P signaling in the same endomembrane system.

DISCUSSION

Using a rigorous set of genetic and biochemical criteria, we identify NPPMs as the first validated Sec14-directed inhibitors, and establish PITPs as pharmacological targets for high resolution dissection of PtdIns-4-P signaling in cells. Our findings emphasize the exquisite PITP selectivities of NPPMs, and demonstrate these compounds do not exert their effects via non-specific membrane-active mechanisms. Rather, the data indicate NPPMs load into the Sec14 hydrophobic pocket during a phospholipid exchange cycle, and invade PtdIns- and PtdCho-acyl chain space while simultaneously engaging Sec14 residues essential for PtdCho headgroup coordination. NPPM engagement of Sec14 residues essential for coordinating the PtdCho headgroup rationalizes the PITP-selectivities of NPPMs. Other Sec14-like PITPs do not conserve the PtdCho headgroup coordinating substructure (Supplementary Fig. 25), and therefore lack the structural elements required for NPPM binding. In this regard, Sfh1 presents a conundrum as it is highly homologous to Sec14 and conserves the functional PtdCho-coordinating unit critical for NPPM binding. Subtle differences in Sec14 vs Sfh1 pocket geometry likely account for the NPPM-resistance of Sfh1. However, given Sec14-like PITPs conserve the PtdIns-binding 'barcode'[10,18], the structural engineering of these proteins also offers prospects for development of broad range inhibitors which survey the PtdIns-headgroup binding site.

The chemical properties of activated aryl halides suggest several mechanisms for how NPPMs inhibit Sec14 activity. One involves aromatic nucleophilic substitution[39], but the potency vector of the *ortho*-halide NPPM series excludes such mechanisms. Rather, we favor non-covalent halogen bonding mechanisms[40,41] (Fig. 6a). Halogen bond interactions require formation of an electropositive 'σ-hole' on the charge surface of the halogen. This

Author Manuscript Author Manuscript Author Manuscript Author Manuscript

organization is enhanced by vicinal *e*- withdrawing groups (e.g. -NO_2), and by propensities of larger halide atoms to adopt anisotropic distributions of electrostatic potentials[41,42]. Correlations of Sec14-active NPPM potencies with electrostatic surface potentials of cognate activated aryl halides support halogen bonding mechanisms for NPPM-mediated Sec14 inhibition. Our calculations project NPPM activated aryl halides form σ-holes, and that σ-hole magnitudes are inversely proportional to halide electronegativity (Fig. 6a). This relationship is congruent with experimentally determined NPPM potencies as Sec14 inhibitors. We propose NPPM occupancy in the Sec14 pocket is anchored by S_{173} engagement with *ortho*-halide via halogen bond, NO_2-group engagements with Y_{111} and Y_{151}, H-bond interaction of the ketone with S_{201}, and intercalation of the NPPM fluorobenzene between F_{228} of the helical gate and F_{212}/M_{177} of the pocket floor (Fig. 6b, c). Proof of a halogen-bonding mechanism requires structural data, however, as the cardinal signature is a 'short' halide-oxygen bond whose length is less than the sum of the halide and oxygen van der Waals radii[40–42].

How does non-covalent NPPM binding in the Sec14 pocket exert a poorly reversible inhibition of PITP activity? NPPM-mediated bridging of the pocket floor to gate sub-structures might tether these elements too strongly for Sec14 to spring the gate for ligand exchange upon membrane association. Alternatively, Sec14-active NPPMs may decouple conformational switch elements required for gate opening by disturbing H_2O networks that lubricate the pocket surface[43] -- thereby locking Sec14 in a 'closed' NPPM-bound state.

The availability of powerful yeast genetic technologies notwithstanding, we forecast significant utility for Sec14-active NPPMs as tool compounds. For example, these SMIs circumvent the tedium of incorporating *sec14*^{ts} mutations into large sets of isogenic yeast strains for running genome-scale screens. Sec14-active SMIs also enable manipulation of in vitro membrane trafficking assays reconstituted with wild-type components – a significant advantage given productive exploitation of genetic tools in cell-free systems is often frustrated by misbehavior of mutant biochemical fractions.

Finally, as PITPs are ubiquitously distributed across the *Eukaryota*[44], PITP-directed screening platforms offer new applications for drug discovery. Because expression of heterologous Sec14-like proteins, or structurally-unrelated mammalian StART-like PITPs, rescue Sec14 defects in yeast[45], such platforms can be purposed for discovery of SMIs directed against target PITPs derived from many biological sources. PITP inhibitors, whether directed against Sec14-like or StART-like PITPs, will enable study of phosphoinositide signaling in organisms intractable to genetic approaches. Many such organisms are significant pathogens. In that regard, we have identified new classes of PITP-directed SMIs that inhibit dimorphic transitions of pathogenic fungi – i.e. inhibit the developmental processes essential to success of these organisms as infectious agents.

ONLINE METHODS

Statistical analyses

Curve fitting and t-test were performed using GraphPad Prism version 5.00 for Windows, GraphPad Software, La Jolla California USA (www.graphpad.com) unless otherwise noted.

Author Manuscript Author Manuscript Author Manuscript Author Manuscript

General data handling was carried out in Excel 2010 (v14.0.4734.1000, 32-bit; Microsoft Corporation). Statistical comparisons of [^{3}H]-PtdIns transfer activities and growth inhibition were calculated using the "extra sum-of-squares F-test" in Graphpad prism v 5.00.

Molecular graphics and chemical drawing

Molecular graphics and analyses were performed with the UCSF Chimera package (version 1.8; http://www.cgl.ucsf.edu/chimera/). Chemical structures in main figures were constructed using ChemBioDraw (PerkinElmer, Cambridge, MA). Chemical structures, substructures and reactions in Supplementary Figures were drawn and displayed using Marvin (5.10.0 and 5.11.4, 2012) and ChemAxon (http://www.chemaxon.com). Docking poses and cavity surfaces were generated using MOE suite (2011.10; Chem. Comp. Group Inc., Montreal, Canada).

Yeast strains, media and reagents—Yeast media and transformation methods are described [46]. Restriction endonucleases were from New England Biolabs (Ipswich, MA), standard reagents from Sigma (St. Louis, MO) or Fisher Scientific (Norcross, GA), and all phospholipids were purchased from Avanti Polar Lipids Inc. (Alabaster, AL). [^{35}S]-Translabel was purchased from MP Biomedicals (Irvine, CA). Yeast strain genotypes are listed in Supplementary Table 1 and plasmids in Supplementary Tables 2 and 3.

Growth rate analyses

Growth assays were conducted in 96 well microtiter plates. In Supplemental Figures 1 and 3a, optical densities were measured every 15 min over the course of 20 hours using a GENios microplate reader (Tecan). All other growth rates were determined as follows. Cells were cultured to mid-logarithmic growth phase in YPD medium (2% glucose) and diluted to λ_{600nm}=0.1 in media appropriately supplemented with SMI or DMSO. Cultures were incubated in 96 well plates in a final volume of 250µl of YPD (2% glucose) for 10–16 hours between 30°C and 32°C. ODs were measured every 15 min. at λ_{610nm} (BioTek Synergy 2) or λ_{595nm} (PerkinElmer VictorX3 3030 Multilabel Plate Reader). Doubling times were calculated and normalized to an internal DMSO control. Nonlinear regression was applied to the dataset to calculate the best fit equation using [Y=100/(1+10^((LogIC$_{50}$−X)*HillSlope))] in Graphpad Prism v5.0. IC$_{50}$ values represent the 95% confidence interval from at least three independent experiments unless otherwise noted. Statistical comparison of SMI-mediated growth inhibition were determined using the "extra sum-of-squares F-test" in Graphpad prism v 5.00.

Site-directed mutagenesis

Site-directed mutations were generated using QuickChange™ (Stratagene) as recommended by the manufacturer. Primer sequences are available from the authors by request.

Small molecule inhibitors—The compounds shown in Supplementary Figure 1 were from ChemDiv (San Diego, CA). SMIs BBV34896-755, BBV34846-244, Z1082669-326, BBV34846-247, BBV34847-734 were synthesized by UORSY/Ukrorgsyntez Ltd. (Riga Latvia). Unless otherwise noted, all other compounds were purchased from ChemBridge Chemical Store, San Diego, CA (www.hit2lead.com). SMIs were dissolved in DMSO

Author Manuscript Author Manuscript Author Manuscript Author Manuscript

(Fisher, D128-500) to a final stock concentration of 20mM and stored in the dark at room temperature. Quality control ^{1}H NMR spectra and LC-MS data are provided in the Supplementary note.

Chemogenomic screening

Pools of bar-coded homozygous and heterozygous deletion strains were grown in YPD + 25mM HEPES (pH 6.8) supplemented with 4130-1278 (35.5μM) and 4130-1276 (6.7μM) for 5 and 20 generations, respectively. Genomic DNA extraction, PCR amplification of molecular barcodes, Genflex tag16k array hybridization/scanning (Affymetrix), and analysis of chemogenomic data are described[19]. Quantile normalized fluorescence values for each tag were $\log_2$-transformed, and z-scores calculated: Tag z-score = [(average of controls)−(experimental value)]/(std. dev. of controls); where the controls were 12 replicate samples of pools treated with DMSO. The z-score for each strain is the average of the 2 tags associated with that strain, and represents the sensitivity value.

NPPM chemogenomic interactions

Interactions were described according to their Gene Ontology (GO) descriptors[47]. Data sets from chemogenomic profiling were analyzed and enriched gene sets were chosen that had Z-scores greater than 4. Gene-sets that did not pass this enrichment threshold are not shown.

Protein purification

Recombinant proteins were purified as described[10]. In summary, pET28b-His_8-Sec14, pET28b-His_8 -Sfh1, pET28b-His_8 –Sfh3 and pET28b-His_8–Sfh4 were grown in *E.coli* BL21 (DE3; New England BioLabs Inc, Ipswich, MA). Sfh2 and Sfh5 expression was driven by pQE30-His_6-Sfh2 and pQE30-His_6-Sfh5 vectors in *E.coli* strain KK2186[25]. Recombinant proteins of interest were bound to TALON metal affinity beads (Clontech, Mountain View, CA), and eluted with imidazole (10mM–200mM gradient) and dialyzed (Prod # 68100, Thermo Scientific, Rockford, IL). In the case of Sec14, dialysis was against 300mM NaCl, 25mM Na_2HPO_4 (pH=7.5), 5mM β-mercapthoethanol. Purified Sfh proteins were dialyzed against the same buffer with the exception that 50mM Na_2HPO_4 was used. Proteins mass was quantified by SDS-PAGE with BSA standard and A_{280}.

PtdIns-transfer assays

[^{3}H]-PtdIns-transfer assays were performed using established methods[10]. In assays involving SMI, purified recombinant PITP was pre-incubated in the presence of acceptor membranes, buffer (300mM NaCl, 25mM Na_2HPO_4, pH 7.5) and SMI for 30 min. at 37°C prior to initiating the assay by addition of radiolabeled donor membranes. Fractional transfer of [^{3}H]-PtdIns was normalized to mock DMSO controls. Nonlinear regression was applied to the dataset to calculate the best fit equation using [Y=100/(1+10^((LogIC$_{50}$−X)*HillSlope))] in Graphpad Prism v5.0. Statistical comparisons of inhibition was calculated using “extra sum-of-squares F-test” in Graphpad prism v 5.00.

Author Manuscript Author Manuscript Author Manuscript Author Manuscript

Metabolic labeling and immunoprecipitation

Strains were grown in minimal media lacking methionine and cysteine to mid-logarithmic phase (OD_{600nm} ~ 0.5). Where indicated, cultures were treated with 20μM SMI or shifted to 37°C for 2h and radiolabeled with 20μCi/ml [^{35}S]-amino acids (Translabel; MP Biomedicals). Chase was initiated by addition of unlabeled methionine and cysteine (2 mM each, final concentration) and terminated with trichloroacetic acid (5% wt/vol, final concentration). CPY immunoprecipitation, SDS-polyacrylamide gel electrophoresis (PAGE), and autoradiography were performed as described[48]. In washout experiments, cultures were pulse-radiolabeled and subjected to chase. Cells were then pelleted (30sec at 4,000rpm), washed 2X with fresh YPD medium, resuspended in YPD containing cyclohexamide (100μg/ml), and further incubated for the indicated times at 30°C. Subsequently, cells were poisoned with trichloroacetic acid (5% wt/vol, final concentration) and samples further processed as described above.

Phosphoinositide analyses

Samples were prepared as described [32,33]. Strain CTY100 (*sec14-1^{ts}*, *sac1*Δ) was grown overnight in uracil-free minimal media containing 2% glucose, 1% case amino acids and labeled to steady state for at least 20h with 10μCi/ml [^{3}H]-*myo*-inositol (ART 0116A; American Radiolabeled Chemicals Inc., St. Louis, MO). Cells were either shifted to 37°C, or challenged with NPPM or DMSO vehicle for 3h, as appropriate. Labeling was terminated with trichloroacetic acid (5% final concentration) and samples incubated on ice for 30 min. Cells were pelleted (10,000 rpm for 1 min), washed twice in 500μl of cold ddH_2O, and resuspended in 500μl 4.5% perchloric acid. Approximately, 300μl of 0.5mm glass beads were added and cells disrupted by vigorous agitation for 10 min in 1 min bursts with 1 min rest on ice.

In experiments where inositol-glycerophospholipids were deacylated and resolved by strong anion exchange HPLC, bulk lipids were extracted as previously described with modification[49]. Bulk lipids were extracted in 2x 250μl of CH_3CH_2OH:ddH_2O:$(C_2H_5)_2O$:C_4H_9OH (15:15:5:1 vol/vol), dried under N_2 gas, and deacylated by resuspension in 300μl of CH_3OH:ddH_2O: C_4H_9OH:CH_3NH_2 (0.8:0.6:0.2:0.35 vol/vol) and incubation for 30 min. at 53°C [50]. 100μl of cold $CH_3CH_2CH_2OH$ was added to the solution, the liquid centrifuged to dryness under vacuum, and dessicate resuspended in 400μl ddH_2O. The solution was extracted 2X with 750μl 1-butanol:petroleum ether:ethyl formate (20:4:1 v/v/v), adjusted to 10mM $(NH_4)_3PO_4$, (pH 3.5), and soluble glycero-phosphoinositols resolved and quantified by HPLC.

In experiments where phosphoinositides were quantified by thin layer chromatography, lysates from disrupted cells was collected and centrifuged at 13,000 rpms for 10 min., the pellet washed with 500μl of 100mM EDTA (pH 7.4), and resuspended in 500μl of $CHCl_3$:CH_3OH:HCL (2:1:0.007). A two-phase system was produced by addition of 100μl of 0.6M HCl, the sample vortexed for 5 min., and sample centrifuged for 5 min. (13,000 rpm). The organic phase was collected, washed 2X with 250μl of CH_3OH:0.6M HCl:$CHCl_3$ (1:0.94:0.06), dried under N_2 gas and resuspended in 50μl $CHCl_3$. Samples were resolved by thin layer chromatography on Partisil LK6DF 60Å silica gel plates (Whatman, Cat#

Author Manuscript Author Manuscript Author Manuscript Author Manuscript

4866-821) using a $CHCl_3$:CH_3OH:ddH_2O:NH_4OH (1:0.83:0.15:0.1) solvent system. Lipids were visualized by autoradiography and quantified with ImageJ (version 1.47t, National Institute of Health).

[^{3}H]-Serine labeling of yeast

[^{3}H]-Serine radiolabeling of yeast was performed as described[13]. The indicated strains were grown overnight at 30°C in uracil- and serine-free minimal media containing glucose (3%), ethanolamine (2mM), and sub-cultured to a λ_{600nm}=0.3. Cells were metabolically radiolabeled for 3h with 3.33μCi/ml L-[3-^{3}H]-serine (ART 0246; American Radiolabeled Chemicals Inc., St. Louis, MO), and either shifted to 37°C, or challenged with 6748-481 (20μM) or DMSO for 3h, as appropriate. Labeling was terminated upon addition of ice-cold trichloroacetic acid (10% final concentration), and samples were incubated on ice for 30 min. Pellets were washed 2X with cold ddH_2O and re-suspended in ddH_2O:absolute ethanol (1:4, v/v) at 100°C for 45 min. The aqueous phase was re-extracted with $CHCl_3$:CH_3OH: 0.2M KCl (4:4:3.3 v/v/v). The organic phase was washed 2X with PBS: CH_3OH (9:10, v/v), dried under N_2 gas, and the lipid film re-suspended in $CHCl_3$:CH_3OH (2:1, v/v) with 1mg/ml of butylated hydroxytoluene. Lipids were resolved by Silica Gel H thin layer chromatography (Analtech, Newark, DE) in a $CHCl_3$:2-propanol:0.25% KCl:triethylamine (30:9:6:18, v/v/v/v) solvent system. Plates were sprayed with 0.2% (w/v) 8-anilino-1-napthalenesulfonic acid, and lipids visualized under UV illumination. Individual lipid species were identified by internal standards (Avanti), collected, and radioactivity quantified by liquid scintillation counting. Sample loads were normalized by total cpm.

Homology modeling of the Sec14 closed conformer

A homology model for the closed Sec14 conformer was generated using Modeller[51] based on the templates of the open conformer of Sec14 (PDB ID 1AUA) [52] and the closed conformer of Sfh1 bound to PtdIns (PDB ID 3B7N) [10]. Gate residues in the Sec14 open conformation (I_{215} – Y_{247}) were removed from that template structure prior to modeling whereas the corresponding gate residues in the closed conformation in Sfh1/PtdIns were retained. In addition, residues A_{84} – Q_{111} on the far side of the binding pocket from the gate were removed from the Sfh1 template prior to modeling since they were structurally divergent from the corresponding Sec14 residues.

Docking simulations

Several independent docking platforms were used. These included; GOLD [CCDC][53]; Glide[54]; QM Polarized Ligand Docking [QM-PLD][55]. Details are presented below.

GOLD docking

Computational docking used the genetic algorithm-based ligand docking program GOLD (version 3.0.25)[53]. GOLD exhaustively explores ligand conformations and provides limited flexibility to protein side chains with -OH groups by reorienting the H-bond donor and acceptor groups. GOLD scoring function is based on favorable conformations found in Cambridge Structural Database, and on empirical results of weak chemical interactions. The active site was defined by a single solvent accessible point near the center of the protein

Author Manuscript Author Manuscript Author Manuscript Author Manuscript

active site, a radius of ~10 Å, and the GOLD cavity detection algorithm. GOLD docking was unconstrained to obtain unbiased results and to explore all possible ligand binding modes. Ligand was docked in independent runs, 50 solutions were produced for each run, (except for one where 20 were generated), as opposed to the default of 10, and early termination of ligand docking was switched off. All other parameters were defaults. All ligands were docked using the same parameters.

Hydropathic scoring

HINT (Hydropathic INTeractions) scoring function was used to analyze docking solutions (version 3.11S b)[56,57]. HINT evaluates each atom-atom interaction in a biomolecular complex using a parameter set derived from solvation partition coefficients for 1-octanol/water. The thermodynamic parameter Log $P_{o/w}$ is directly correlated with free energy. HINT describes specific interactions between two molecules as:

$$B=\sum\sum b_{ij}=\sum\sum (a_i S_i a_j S_j R_{ij} T_{ij}+r_{ij})$$

where a is the hydrophobic atom constant derived from $Log_{o/w}$, S is the solvent accessible surface area, T is a function that differentiates polar-polar interactions (acid–acid, acid–base or base–base), and R, r are functions of the distance between atoms i and j as previously described [57]. The binding score, b_{ij}, describes the specific atom–atom interaction between atoms i and j, whereas B describes the total interaction. For selection of the optimum docked conformation and to further differentiate the relative binding efficacy of the NPPM ligands, interaction scores were calculated for each pose found by docking. The protein and ligands were partitioned as distinct molecules. ‘Essential’ hydrogen atoms, that is, only those attached to polar atoms (N, O, S, P), were explicitly considered in the model and assigned HINT constants. The inferred solvent model, where each residue is partitioned based on its hydrogen count, was applied. The solvent accessible surface area for the amide nitrogens was corrected with the ‘+20’ option.

Glide docking

Protein and ligands were prepared using Protein Preparation Wizard and LigPrep module of Maestro 9.2 Interface of Schrodinger Suite (Schrodinger Suite 2012; Glide version 5.8). Receptor Grids were generated without using any constraints and standard settings were used. Docking was performed using Standard Glide and QM-PLD modules with SP and XP scoring function respectively. No similarity, torsional and inter-molecular interaction (hydrogen bonding or hydrophobic) constraints were used. Ligand was docked flexibly with nitrogen inversions and ring sampling turned on with post-docking minimization.

PLIF

Protein-Ligand Interaction Fingerprint (PLIF) was calculated within MOE suite (2011.10; Chem. Comp. Group Inc., Montreal, Canada). PLIF was calculated between a closed Sec14 conformer and 6 representative binding modes produced by the docking runs. The protein Ligand Interaction Fingerprint (PLIF) is a method to encapsulate the interaction between ligands and proteins using a fingerprint scheme. To generate PLIF within MOE, maximum

Author Manuscript Author Manuscript Author Manuscript Author Manuscript

250 bits were used with Min Score 1 turned off and keeping the Min Score 2 to its default value.

Simulation of charge distribution on activated aryl halides

Wave function calculations were carried out using the PC Spartan package (Wavefunction Inc. Irvine, CA; version 10 1.1.0). Starting geometries were obtained using Spartan's interactive building mode, and pre-optimized using the MMFF force field. Wave functions were approximated using the Hartree-Fock method at the 3–21G$^{(*)}$ gaussian basis set. Electrostatic potentials were generated onto surfaces of molecular electron densities (0.002 electrons per A^3).

Fluorescence imaging

N-[3-Triethylammoniumpropyl]-4-[*p*-diethylaminophenylhexatrienyl] pyridinium dibromide (FM4-64; Invitrogen, Carlsbad, CA) staining was performed as described below. Cells were grown to mid-logarithmic phase ($OD_{600\ nm}$=0.5) in YPD medium at 30°C, then either shifted to 37°C for 2h or treated with 20μM SMI at 25°C for 2 h. Subsequently, cells were pulsed with 10μM FM4-64 (Invitrogen) for 15 min. washed 2X in YPD media matched to the appropriate drug or temperature condition. Labeling was terminated at indicated times by washing cells in NaN_3/NaF (1mM final concentration of each) and placing samples on ice prior to imaging.

Cultures for GFP-Snc1 imaging were grown in synthetic defined medium lacking uracil at 30°C. Cells processed for imaging of phosphoinositide biosensors were collected from liquid cultures grown in uracil-free YNB supplemented with 3% glucose and 1% casamino acids at 25°C by centrifugation at 4,000 rpm for 1 min, and resuspended into fresh uracil-deficient medium prior to analysis. Cells were immobilized onto a thin layer of growth medium with 20% gelatin (G-2500, Sigma-Aldrich), sealed under a coverslip with Valap, and examined at 25°C. The imaging system employed a CFI plan apochromat lambda 100x oil immersion objective lens NA 1.45 mounted on a Nikon Ti-U microscope base (Nikon, Melville, NY) interfaced to a Photometrics CoolSNAP HQ2 high sensitivity monochrome CCD camera (Roper Scientific, Ottobrunn, Germany) or an Andor Neo sCMOS CCD camera (Andor Technology, Belfast, UK). A Lumen 200 Illumination System (Prior Scientific Inc., Rockland, MA.) was used in conjunction with a B-2E/C (465–495nm/515–555nm;EX/EM) or G-2E/C (528–553nm/590–650nm;EX/EM) filter set (Nikon, Melville, NY). Images were captured using the Nikon NIS Elements software package (Nikon, Melville, NY, version 4.10) and exported as .TIF files. Image analyses were performed using ImageJ (version 1.47t, National Institute of Health) and figures were constructed using Adobe Illustrator and Adobe Photoshop CS6 (version 15.0.0).

Transmission electron microscopy

Yeast were grown to an $OD_{600\ nm}$=0.5 and cultures were either shifted to 37°C for 2 hours or challenged with 20μM SMI for 2 hours at 30°C. Cells were fixed in 3% glutaraldehyde, converted to spheroplasts, stained with 2% OsO_4 and 2% uranyl acetate, dehydrated in a 50%, 70%, 90% ethanol series, and washed in 100% ethanol and 100% acetone, respectively. Cell pellets were embedded into Spurr's resin at 60°C for 48h and sectioned[58].

Author Manuscript Author Manuscript Author Manuscript Author Manuscript

Thin sections produced from strains in the *SEC14*$^{p\text{-}136}$ (CTY374) background were imaged at 80 kV on a Tecnai 12 electron microscope (FEI, Hillsboro, OR), and images captured using Gatan micrograph with version 3.9.3 software (Gatan, Pleasanton, CA). All other samples were visualized on a Jeol 1200 EX TEM operated at an accelerating voltage of 100 kV. Images were captured at calibrated magnifications using an optically coupled 3k slow scan CCD camera (model 15C, SIA, Duluth, GA) and Maxim DL imaging software.

Invertase secretion assays

Cells were grown in YPD (2% glucose) at 30°C, cultures were split, and cells incubated at 30°C ± NPPM (20μM) or DMSO or 37°C for 1h in YPD (2% glucose). Cells were then pelleted (2000g), washed twice with pre-warmed YPD (0.1% glucose), resuspended in the low glucose YPD medium, and incubated as before for 1.5h. To halt trafficking, samples were adjusted to 10mM NaN_3, and incubated on ice. The samples were washed 3X with 500μl ice-cold 10mM NaN_3 and re-suspended in 500μl of the same. The samples were split into 10mM NaN_3 buffers ± 0.2 % Triton X-100 (final) with the Triton-solubilized fractions also being subjected to one cycle of freeze-thaw to generate the permeabilized cell fraction. The partner non-permeabilized and permeabilized samples were used to determine extracellular and total invertase activities, respectively[59]. Invertase units were expressed as nmoles of glucose produced per min. at 30°C.

Sequence alignment

Protein sequences were acquired from the Universal Protein Resource, aggregated using UGENE (version 1.10.1; http://ugene.unipro.ru/), and aligned with the T-Coffee module using the default settings. Homologous sequences were superimposed onto structural models (PDB IDs 1AUA, 1OLM, 3B7Z, 4FMM) to highlight the PtdIns/PtdCho lipid binding barcode.

Supplementary Material

Refer to Web version on PubMed Central for supplementary material.

Acknowledgments

This work was supported by the Robert A. Welch Foundation (VAB) and grant GM44530 (VAB) from the NIH. RWD was supported by the NIH (HG003317). G. Giaever and C. Nislow were supported by the NHGRI (5RO1-003317-08) and the Canadian Cancer Society (020380). The Texas A&M Laboratory for Molecular Simulation provided software, support and computer time. Glen E. Kellogg and eduSoft LC donated HINT software, Ulrich Schlecht (Stanford) assisted with growth analyses, Andreas Holzenburg and Richard Littleton (Texas A&M) assisted with electron microscopy. We are grateful to Daniel Lew (Duke) for donating *mss4*^{ts} alleles.

References

1. Wymann MP, Schneiter R. Lipid signalling in disease. Nat Rev Mol Cell Biol. 2008; 9:162–176. [PubMed: 18216772]
2. Janmey PA, Lindberg U. Cytoskeletal regulation: rich in lipids. Nat Rev Mol Cell Biol. 2004; 5:658–66. [PubMed: 15366709]
3. Henry SA, Kohlwein SD, Carman GM. Metabolism and regulation of glycerolipids in the yeast Saccharomyces cerevisiae. Genetics. 2012; 190:317–49. [PubMed: 22345606]
4. Irvine RF. Nuclear lipid signalling. Nat Rev Mol Cell Biol. 2003; 4:349–60. [PubMed: 12728269]

Author Manuscript Author Manuscript Author Manuscript Author Manuscript

5. Di Paolo G, De Camilli P. Phosphoinositides in cell regulation and membrane dynamics. Nature. 2006; 443:651–657. [PubMed: 17035995]
6. Michell RH. Inositol derivatives: evolution and functions. Nat Rev Mol Cell Biol. 2008; 9:151–61. [PubMed: 18216771]
7. Strahl T, Thorner J. Synthesis and function of membrane phosphoinositides in budding yeast, Saccharomyces cerevisiae. Biochim Biophys Acta. 2007; 1771:353–404. [PubMed: 17382260]
8. Varnai P, Thyagarajan B, Rohacs T, Balla T. Rapidly inducible changes in phosphatidylinositol 4,5-bisphosphate levels influence multiple regulatory functions of the lipid in intact living cells. J Cell Biol. 2006; 175:377–82. [PubMed: 17088424]
9. Suh BC, Inoue T, Meyer T, Hille B. Rapid chemically induced changes of PtdIns(4,5)P_2 gate KCNQ ion channels. Science. 2006; 314:1454–7. [PubMed: 16990515]
10. Schaaf G, et al. Functional Anatomy of Phospholipid Binding and Regulation of Phosphoinositide Homeostasis by Proteins of the Sec14 Superfamily. Mol Cell. 2008; 29:191–206. [PubMed: 18243114]
11. Bankaitis VA, Mousley CJ, Schaaf G. The Sec14 superfamily and mechanisms for crosstalk between lipid metabolism and lipid signaling. Trends Biochem Sci. 2010; 35:150–160. [PubMed: 19926291]
12. Bankaitis VA, Malehorn DE, Emr SD, Greene R. The Saccharomyces cerevisiae SEC14 gene encodes a cytosolic factor that is required for transport of secretory proteins from the yeast Golgi complex. J Cell Biol. 1989; 108:1271–81. [PubMed: 2466847]
13. Wu WI, Routt S, Bankaitis VA, Voelker DR. A new gene involved in the transport-dependent metabolism of phosphatidylserine, PSTB2/PDR17, shares sequence similarity with the gene encoding the phosphatidylinositol/phosphatidylcholine transfer protein, SEC14. J Biol Chem. 2000; 275:14446–56. [PubMed: 10799527]
14. Desfougères T, Ferreira T, Bergès T, Régnacq M. SFH2 regulates fatty acid synthase activity in the yeast Saccharomyces cerevisiae and is critical to prevent saturated fatty acid accumulation in response to haem and oleic acid depletion. Biochem J. 2008; 409:299–309. [PubMed: 17803462]
15. Vincent P, et al. A Sec14p-nodulin domain phosphatidylinositol transfer protein polarizes membrane growth of Arabidopsis thaliana root hairs. J Cell Biol. 2005; 168:801–12. [PubMed: 15728190]
16. Lopez MC, et al. A phosphatidylinositol/phosphatidylcholine transfer protein is required for differentiation of the dimorphic yeast Yarrowia lipolytica from the yeast to the mycelial form. J Cell Biol. 1994; 125:113–27. [PubMed: 8138566]
17. Alb JG Jr, et al. Mice lacking phosphatidylinositol transfer protein-alpha exhibit spinocerebellar degeneration, intestinal and hepatic steatosis, and hypoglycemia. J Biol Chem. 2003; 278:33501–18. [PubMed: 12788952]
18. Nile AH, Bankaitis VA, Grabon A. Mammalian diseases of phosphatidylinositol transfer proteins and their homologs. Clin Lipidol. 2010; 5:867–897. [PubMed: 21603057]
19. Hoon S, et al. An integrated platform of genomic assays reveals small-molecule bioactivities. Nat Chem Biol. 2008; 4:498–506. [PubMed: 18622389]
20. Xie Z, et al. Phospholipase D activity is required for suppression of yeast phosphatidylinositol transfer protein defects. Proc Natl Acad Sci USA. 1998; 95:12346–51. [PubMed: 9770489]
21. Kennedy MA, et al. Srf1 is a novel regulator of phospholipase D activity and is essential to buffer the toxic effects of C16:0 platelet activating factor. PLoS Genet. 2011; 7:e1001299. [PubMed: 21347278]
22. Mousley CJ, et al. Trans-Golgi Network and Endosome Dynamics Connect Ceramide Homeostasis with Regulation of the Unfolded Protein Response and TOR Signaling in Yeast. Mol Biol Cell. 2008; 19:4785–4803. [PubMed: 18753406]
23. Curwin AJ, Fairn GD, McMaster CR. Phospholipid Transfer Protein Sec14 Is Required for Trafficking from Endosomes and Regulates Distinct trans-Golgi Export Pathways. J Biol Chem. 2009; 284:7364–7375. [PubMed: 19129178]
24. Salama SR, Cleves AE, Malehorn DE, Whitters EA, Bankaitis VA. Cloning and characterization of Kluyveromyces lactis SEC14, a gene whose product stimulates Golgi secretory function in Saccharomyces cerevisiae. J Bacteriol. 1990; 172:4510–21. [PubMed: 2198263]

Author Manuscript Author Manuscript Author Manuscript Author Manuscript

25. Li X, et al. Identification of a Novel Family of Nonclassic Yeast Phosphatidylinositol Transfer Proteins Whose Function Modulates Phospholipase D Activity and Sec14p-independent Cell Growth. Mol Biol Cell. 2000; 11:1989–2005. [PubMed: 10848624]
26. Schaaf G, et al. Resurrection of a functional phosphatidylinositol transfer protein from a pseudo-Sec14 scaffold by directed evolution. Mol Biol Cell. 2011; 22:892–905. [PubMed: 21248202]
27. Cleves A, McGee T, Bankaitis V. Phospholipid transfer proteins: a biological debut. Trends Cell Biol. 1991; 1:30–4. [PubMed: 14731807]
28. Cleves AE, et al. Mutations in the CDP-choline pathway for phospholipid biosynthesis bypass the requirement for an essential phospholipid transfer protein. Cell. 1991; 64:789–800. [PubMed: 1997207]
29. Li X, et al. Analysis of oxysterol binding protein homologue Kes1p function in regulation of Sec14p-dependent protein transport from the yeast Golgi complex. J Cell Biol. 2002; 157:63–77. [PubMed: 11916983]
30. Fang M, et al. Kes1p shares homology with human oxysterol binding protein and participates in a novel regulatory pathway for yeast Golgi-derived transport vesicle biogenesis. EMBO J. 1996; 15:6447–59. [PubMed: 8978672]
31. Stevens T, Esmon B, Schekman R. Early stages in the yeast secretory pathway are required for transport of carboxypeptidase Y to the vacuole. Cell. 1982; 30:439–48. [PubMed: 6754086]
32. Phillips SE, et al. Yeast Sec14p Deficient in Phosphatidylinositol Transfer Activity Is Functional In Vivo. Mol Cell. 1999; 4:187–197. [PubMed: 10488334]
33. Rivas MP, et al. Pleiotropic alterations in lipid metabolism in yeast sac1 mutants: relationship to “bypass Sec14p” and inositol auxotrophy. Mol Biol Cell. 1999; 10:2235–50. [PubMed: 10397762]
34. Hama H, Schnieders EA, Thorner J, Takemoto JY, DeWald DB. Direct involvement of phosphatidylinositol 4-phosphate in secretion in the yeast Saccharomyces cerevisiae. J Biol Chem. 1999; 274:34294–300. [PubMed: 10567405]
35. Guo S, Stolz LE, Lemrow SM, York JD. SAC1-like domains of yeast SAC1, INP52, and INP53 and of human synaptojanin encode polyphosphoinositide phosphatases. J Biol Chem. 1999; 274:12990–5. [PubMed: 10224048]
36. Wood CS, et al. PtdIns4P recognition by Vps74/GOLPH3 links PtdIns 4-kinase signaling to retrograde Golgi trafficking. J Cell Biol. 2009; 187:967–75. [PubMed: 20026658]
37. Roy A, Levine TP. Multiple pools of phosphatidylinositol 4-phosphate detected using the pleckstrin homology domain of Osh2p. J Biol Chem. 2004; 279:44683–9. [PubMed: 15271978]
38. Baird D, Stefan C, Audhya A, Weys S, Emr SD. Assembly of the PtdIns 4-kinase Stt4 complex at the plasma membrane requires Ypp1 and Efr3. J Cell Biol. 2008; 183:1061–74. [PubMed: 19075114]
39. Sykes, P. A guidebook to mechanism in organic chemistry. 6. Pearson; 1986.
40. Lu YC-X, et al. H contacts in biomolecular systems: how they contribute to protein-ligand binding affinity. J Phys Chem. 2009; 113:12615–21.
41. Auffinger P, Hays FA, Westhof E, Ho PS. Halogen bonds in biological molecules. Proc Natl Acad Sci USA. 2004; 101:16789–94. [PubMed: 15557000]
42. Metrangolo P, Resnati G. Halogen bonding: a paradigm in supramolecular chemistry. Chemistry. 2001; 7:2511–9. [PubMed: 11465442]
43. Ryan MM, Temple BR, Phillips SE, Bankaitis VA. Conformational dynamics of the major yeast phosphatidylinositol transfer protein sec14p: insight into the mechanisms of phospholipid exchange and diseases of sec14p-like protein deficiencies. Mol Biol Cell. 2007; 18:1928–42. [PubMed: 17344474]
44. Phillips SE, et al. The Diverse Biological Functions of Phosphatidylinositol Transfer Proteins in Eukaryotes. Crit Rev Biochem Mol Biol. 2006; 41:21–49. [PubMed: 16455519]
45. Skinner HB, Alb JG Jr, Whitters EA, Helmkamp GM Jr, Bankaitis VA. Phospholipid transfer activity is relevant to but not sufficient for the essential function of the yeast SEC14 gene product. EMBO J. 1993; 12:4775–84. [PubMed: 8223486]
46. Sherman, F.; Fink, GR.; Hink, JB. Methods in Yeast Genetics: A Laboratory Manual. Cold Spring Harbor: 1983.

Author Manuscript Author Manuscript Author Manuscript Author Manuscript

47. Ashburner M, et al. Gene ontology: tool for the unification of biology. The Gene Ontology Consortium. Nat Genet. 2000; 25:25–9. [PubMed: 10802651]
48. Young BP, Craven RA, Reid PJ, Willer M, Stirling CJ. Sec63p and Kar2p are required for the translocation of SRP-dependent precursors into the yeast endoplasmic reticulum in vivo. EMBO J. 2001; 20:262–71. [PubMed: 11226176]
49. Stolz LE, Kuo WJ, Longchamps J, Sekhon MK, York JD. INP51, a yeast inositol polyphosphate 5-phosphatase required for phosphatidylinositol 4,5-bisphosphate homeostasis and whose absence confers a cold-resistant phenotype. Biol Chem. 1998; 273:11852–61.
50. Clarke NG, Dawson RM. Alkaline O leads to N-transacylation. A new method for the quantitative deacylation of phospholipids. Biochem J. 1981; 195:301–6. [PubMed: 7306057]
51. Šali A, Blundell TL. Comparative Protein Modelling by Satisfaction of Spatial Restraints. J Mol Biol. 1993; 234:779–815. [PubMed: 8254673]
52. Sha B, Phillips SE, Bankaitis VA, Luo M. Crystal structure of the Saccharomyces cerevisiae phosphatidylinositol-transfer protein. Nature. 1998; 391:506–510. [PubMed: 9461221]
53. Jones G, Willett P, Glen RC, Leach AR, Taylor R. Development and validation of a genetic algorithm for flexible docking. J Mol Biol. 1997; 267:727–48. [PubMed: 9126849]
54. Friesner RA, et al. Extra precision glide: docking and scoring incorporating a model of hydrophobic enclosure for protein-ligand complexes. J Med Chem. 2006; 49:6177–96. [PubMed: 17034125]
55. Cho AE, Guallar V, Berne BJ, Friesner R. Importance of accurate charges in molecular docking: quantum mechanical/molecular mechanical (QM/MM) approach. J Comptu Chem. 2005; 26:915–31.
56. Meng E, Kuntz I, Abraham D, Kellogg G. Evaluating docked complexes with the HINT exponential function and empirical atomic hydrophobicities. J Comptu Aided Mol Des. 1994; 8:299–306.
57. Abraham DJ, Kellogg GE, Holt JM, Ackers GK. Hydropathic analysis of the non-covalent interactions between molecular subunits of structurally characterized hemoglobins. J Mol Biol. 1997; 272:613–632. [PubMed: 9325116]
58. Adamo JE, et al. Yeast Cdc42 functions at a late step in exocytosis, specifically during polarized growth of the emerging bud. J Cell Biol. 2001; 155:581–592. [PubMed: 11706050]
59. Goldstein A, Lampen JO. Beta-D-fructofuranoside fructohydrolase from yeast. Methods Enzymol. 1975; 42:504–11. [PubMed: 237205]

Author Manuscript Author Manuscript Author Manuscript Author Manuscript

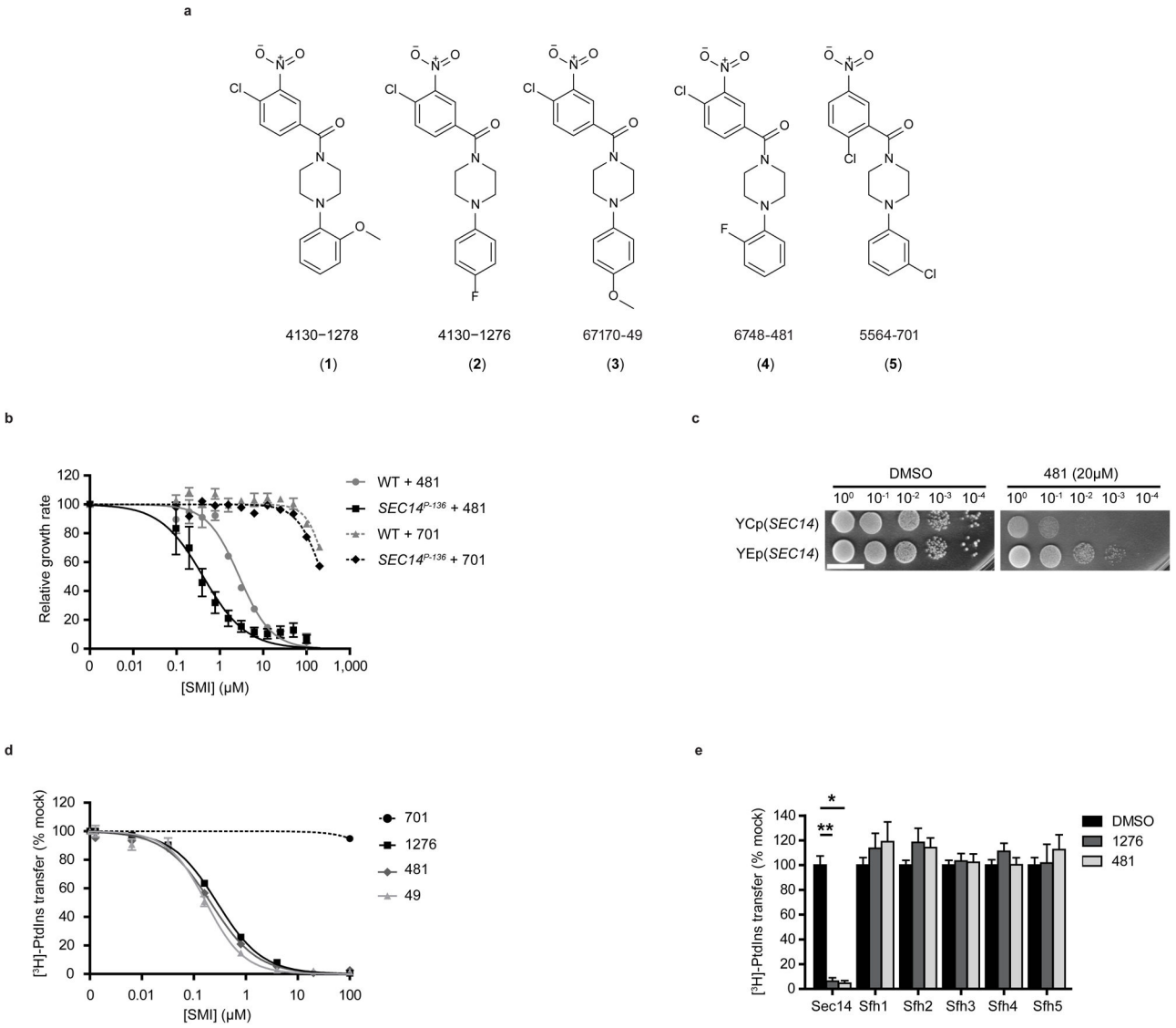

Figure 1. NPPMs specifically inactivate Sec14

(**a**) Chemical structures of 4130-1278, 4130-1276, 67170-49, 6748-481, and 5564-701. (**b**) Growth inhibition of wild-type (WT; CTY182, gray) and *SEC14*$^{P\text{-}136}$ (CTY374; black) strains by 6748-481 (●,■; IC_{50}s=2.87±0.6 and 0.44±0.16μM, respectively) or 5564-701 (▲,◆; IC_{50}s>200μM). Relative growth compares growth rate with compound relative to "no-drug" control (DMSO). Data are plotted as function of NPPM concentration (x-axis). Doubling times were measured at λ_{610nm}. Values show mean ± s.e.m of normalized doubling times for each drug concentration from 3 independent experiments. IC_{50}s represent 95% confidence interval from 3 independent experiments. (**c**) Yeast expressing physiological [YCp(*SEC14*)], or elevated [YEp(*SEC14*)], Sec14 levels were spotted in 10-fold dilution series onto YPD agar with DMSO or 6748-481 (20μM) and incubated at 30°C (48h). Bar, 1cm. (**d**) [^{3}H]-PtdIns-transfer was monitored in vitro using purified Sec14 with 5564-701 (IC_{50}>100μM), 4130-1276 (IC_{50}=283 ± 30nM), 6748-481 (IC_{50}=211 ± 19nM) or 67170-49 (IC_{50}=175 ± 26nM). Relative [^{3}H]-PtdIns transfer relates activity in presence of

Author Manuscript Author Manuscript Author Manuscript Author Manuscript

NPPM relative to vehicle control (DMSO) in assays where Sec14 concentration was clamped (287nM). Values indicate mean ± s.e.m of triplicate determinations from 3 independent experiments. IC_{50} values fall into 95% confidence intervals. [^{3}H]-PtdIns input ranged from 12790–16800 cpm, with background ranging from 478–751 cpm. (**e**) Purified Sfh proteins (10μg) were assayed for [^{3}H]-PtdIns transfer in the presence and absence of indicated NPPM (40μM). Values are the mean ± s.d of triplicate determinations from 3 independent experiments. P*=1.8202E^{-11} and P**=4.31133E^{-12} relative to DMSO control (two-tailed t-test with heteroscedastic variance, Microsoft Excel 2010). [^{3}H]-PtdIns input ranged from 14441–15101 cpm, with background ranging from 640–657 cpm.

Author Manuscript Author Manuscript Author Manuscript Author Manuscript

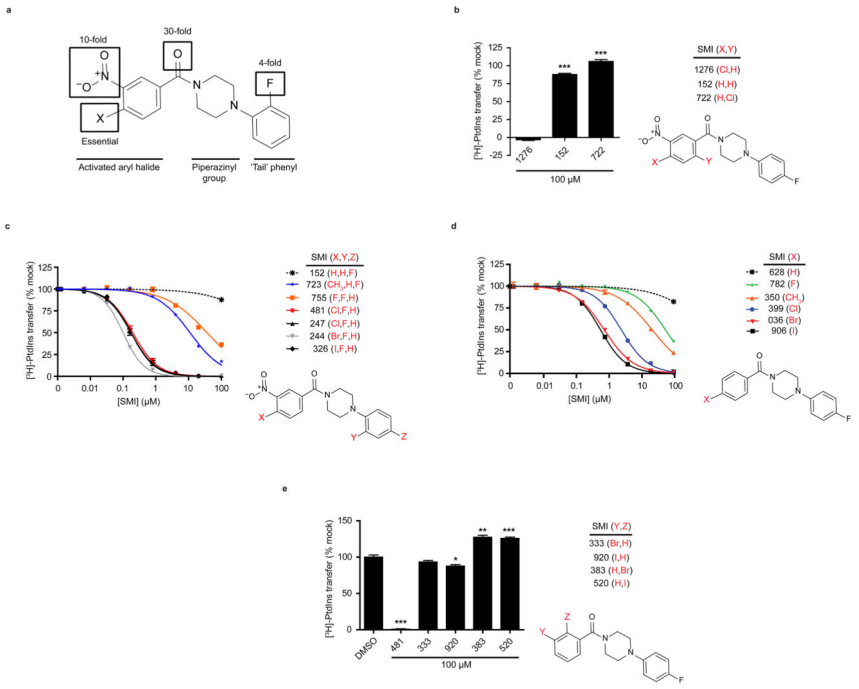

Figure 2. NPPM SAR relationships

(**a**) A summary of the contributions of each highlighted functional group of NPPM 6748-481 to potency as Sec14 inhibitor is depicted. Data represent a compilation, and superimposition onto the 6748-481 scaffold, of IC_{50} measurements for Sec14-catalyzed [^{3}H]-PtdIns transfer activity for each SMI listed in Supplementary Figure 4. (**b–e**) Chemical-induced inhibition of Sec14-catalyzed [^{3}H]-PtdIns transfer activity was monitored in the presence of the indicated SMI. Chemical identities for functional groups X, Y and Z are identified for each SMI tested, and are highlighted in red. Relative [^{3}H]-PtdIns transfer compares activity in presence of compound relative to the “no-drug” control (DMSO) in assays where Sec14 concentration was clamped at 287nM. IC_{50} values: 5355-152 (>100,000 nM),5658-722 (>100,000 nM), 5348-723 (11,060 ± 1,130 nM), 6748-481 (211 ± 19 nM), BBV34896-755 (36,800 ± 5,000 nM), BBV34846-247 (173 ± 35 nM), BBV34846-244 (100 ± 6 nM), Z1082669-326 (174 ± 17 nM), 5356-628 (>100,000 nM), 5567-782 (56,500 ± 7,680 nM), 5356-350 (22,000 ± 3,100 nM), 5357-399 (2,550 ± 230 nM), 5353-036 (768 ± 71 nM), 7329-906 (589 ± 51 nM), 5656-333 (>100,000 nM), 6031-920 (>100,000 nM), 5353-383 (>100,000 nM), 5653-520 (>100,000 nM). [^{3}H]-PtdIns input ranged from 7,542-13,002 cpm per assay, with background ranging from 282-1,317 cpm and transfer efficiency (% of total input) ranged from 11% to 32%. Values indicate the mean ± s.e.m of triplicate determinations from three independent experiments. IC_{50} values represent the 95% confidence interval or for single concentration points a predicted IC_{50}. Statistical comparisons of values used the “unpaired two-tailed t-test” where P***<0.0001, P**=0.0024 and P*=0.0089.

Author Manuscript Author Manuscript Author Manuscript Author Manuscript

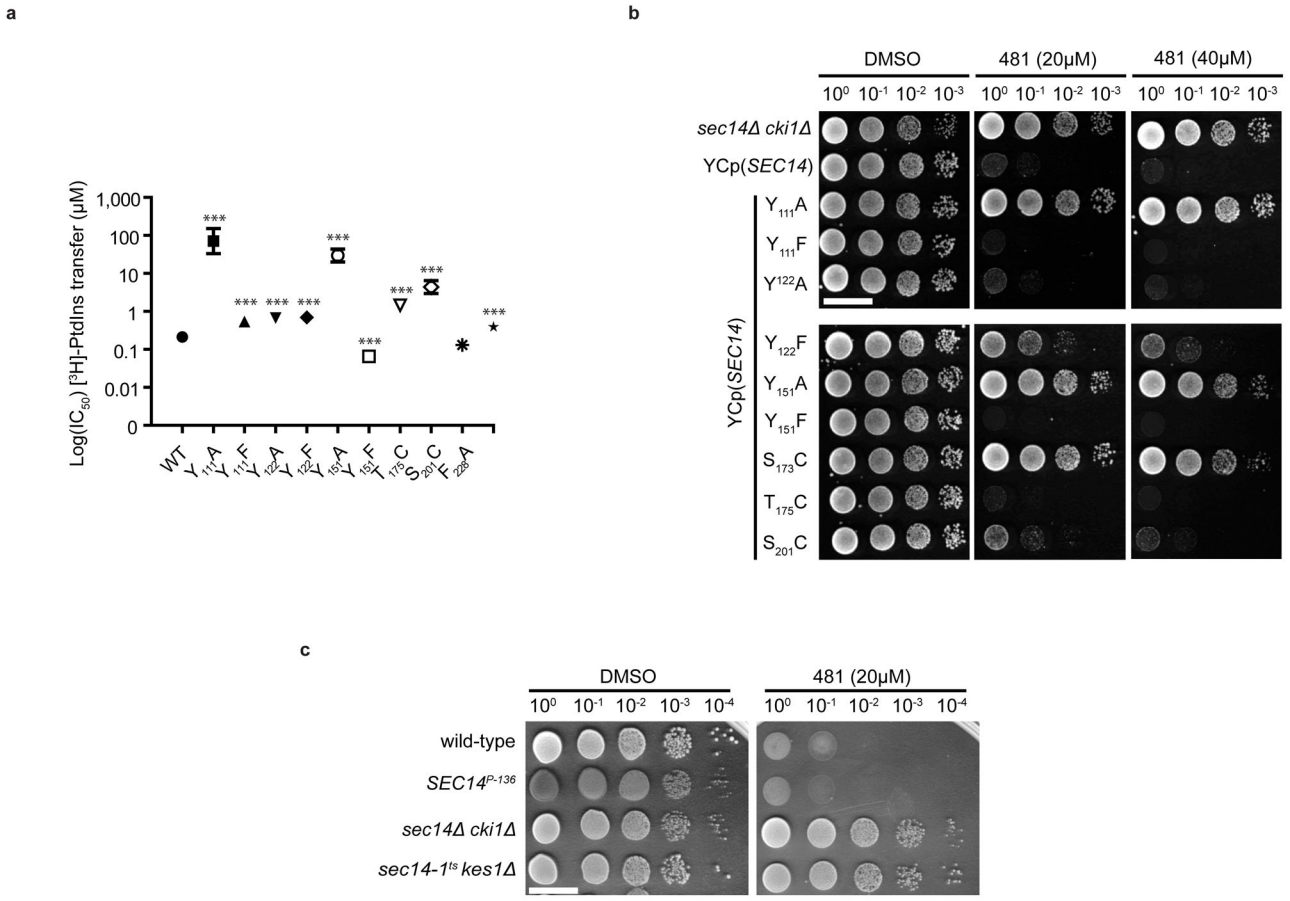

Figure 3. Sec14 is the essential cellular target of bioactive NPPMs

[^{3}H]-PtdIns transfer was measured using purified recombinant Sec14 proteins (287nM) in the presence of 6748-481. (**a**) Relative [^{3}H]-PtdIns transfer compares activities in presence of 6748-481 relative to the "no-drug" control (DMSO). Input ranged from 9,227–16985 cpm per assay (background; 160–724 cpm). Transfer efficiencies: Sec14 (24–32%), Sec14^{Y111A} (5–13%), Sec14^{Y111F} (38–41%), Sec14^{Y122A} (13–15%), Sec14^{Y122F} (18–27%), Sec14^{Y151A} (31–40%), Sec14^{Y151F} (31–40%), Sec14^{S173C} (22–24%), Sec14^{T175C} (5–16%), Sec14^{S201C} (6–11%), Sec14^{M177C} (8–10%), and Sec14^{F228A} (18–27%). IC_{50} values represent 95% confidence interval of triplicate determinations from three independent experiments. Statistical comparisons of WT to mutant IC_{50} values used "extra sum-of-squares F-test" (P***<0.0001). (**b**) Expression of NPPM-resistant Sec14 derivatives renders cells insensitive to NPPM-mediated growth arrest. Yeast expressing physiological levels of Sec14, YCp(*SEC14*), or the indicated Sec14 variant, as the sole source of Sec14 in the cell, were diluted in 10-fold series onto YPD agar containing DMSO, 20μM or 40μM 6748-481. Plates were incubated at 30°C (48h). (**c**) 'Bypass Sec14' mutants are NPPM-resistant. WT (CTY182), *SEC14^{P-136}* (CTY374), and *sec14*Δ *cki1*Δ (CTY303) and *sec14-1^{ts} kes1*Δ (CTY159) 'bypass Sec14' mutants were grown as in (b). Bar, 1cm.

Author Manuscript Author Manuscript Author Manuscript Author Manuscript

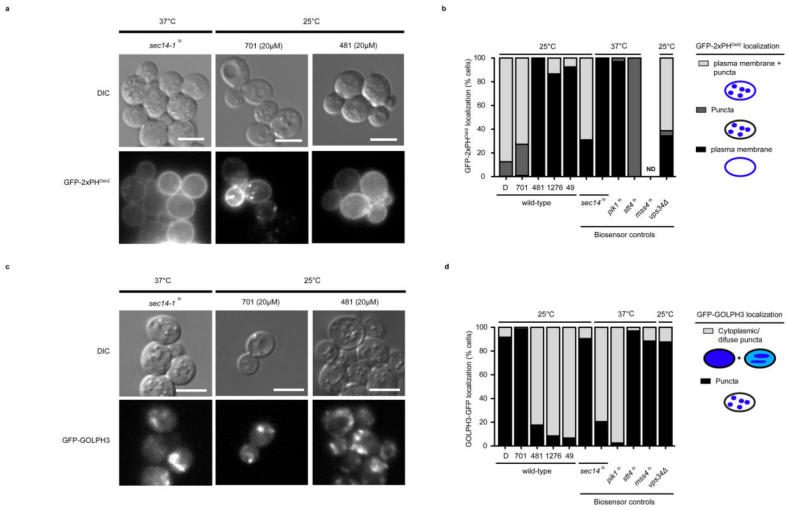

Figure 4. Sec14-active NPPMs exhibit compartment-specific inhibition of PtdIns-(4)-phosphate signaling

(**a**) WT yeast (CTY182) or the indicated temperature sensitive mutants containing GFP-2xPH^{Osh2} were treated with indicated SMIs (20μM) for 3h at 25°C, or 37C. GFP-2xPH^{Osh2} profiles were imaged, and profiles scored. (**b**) GFP-2xPH^{Osh2} distributions were classified as PM, punctate, or both. ND – not determined. At least 300 cells were scored for each condition in (a). (**c**) Experimental conditions were as in (a) except GFP-GOLPH3 distribution was monitored. The *mss4-5^{ts}* mutant was incubated for 30 min. at non-permissive temperature. (**d**) GFP-GOLFP3 distribution was scored (>300 cells for each condition), and GFP-GOLPH3 distributions were classified as PM, punctate, or both. Bar, 5μm.

Author Manuscript
Author Manuscript
Author Manuscript
Author Manuscript

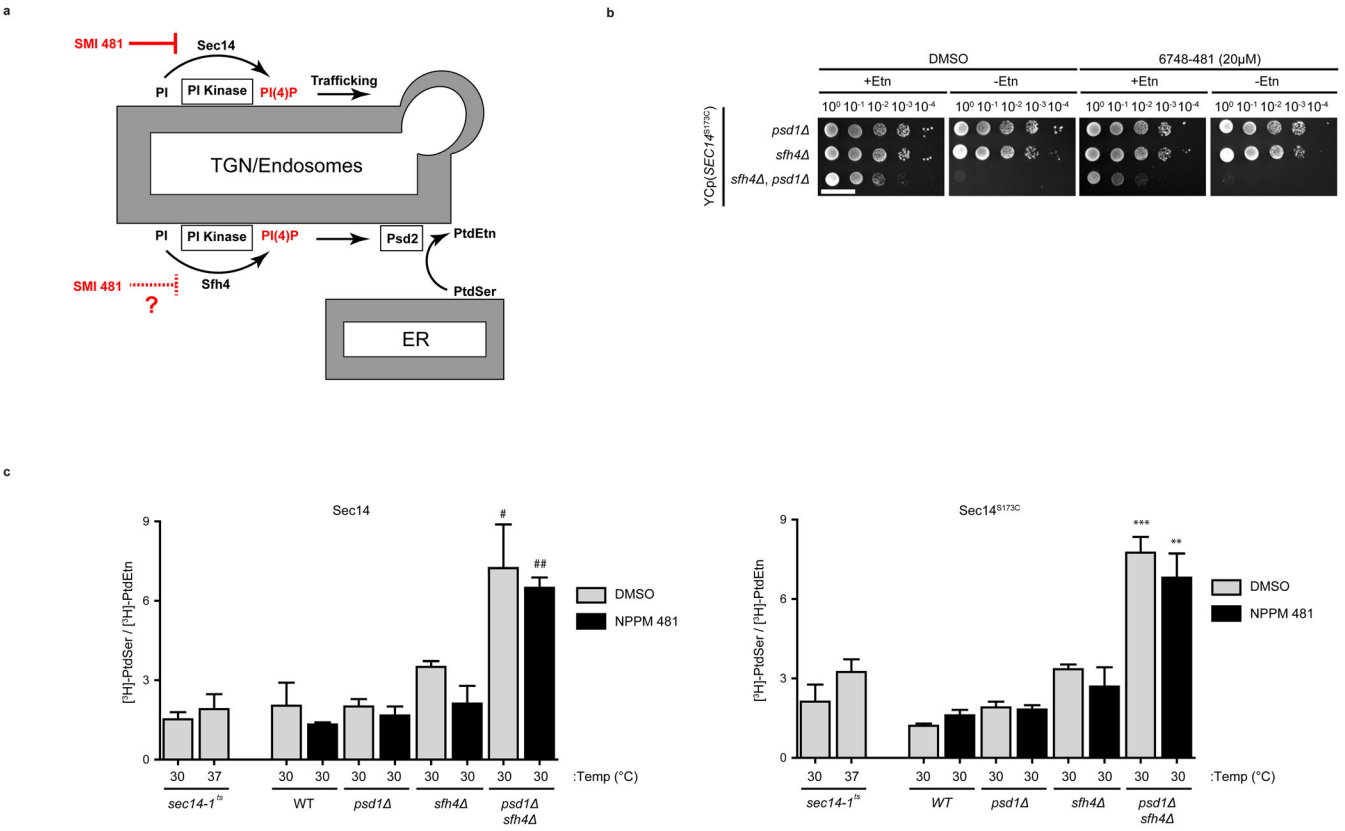

Figure 5. NPPMs discriminate between Sec14- and Sfh4-mediated PtdIns-4-P signaling

(**a**) Sec14 and Sfh4 control distinct PtdIns-4-P signaling pathways in TGN/endosomal compartments. Sec14 couples PtdIns 4-OH kinase action with vesicle biogenesis, whereas Sfh4 pathway couples PtdIns 4-OH kinase action with PtdSer decarboxylation to PtdEtn. Decarboxylation is catalyzed by Psd2 and is posited to involve membrane contact sites that bridge the endoplasmic reticulum (ER) with TGN/endosomes. (**b**) *psd1*Δ (PYY23), *sfh4*Δ (PYY40), or *sfh4*Δ *psd1*Δ (PYY30) yeast expressing the NPPM-resistant Sec14^{S173C} [YCp(*SEC14*^{S173C})] were spotted in 10-fold dilution series on uracil-free agar ± ethanolamine (1mM), with or without 6748-481 (20μM). Plates were incubated at 30°C (96h). (**c**) WT (CTY182), *sec14-1*^{ts} (CTY1-1A), *psd1*Δ (PYY23), *sfh4*Δ (PYY40), or *sfh4*Δ *psd1*Δ (PYY30) cells expressing Sec14 or Sec14^{S173C} were cultured in uracil-free media containing ethanolamine (2mM) at 30°C. Mid-logarithmic growth phase cultures (λ_{600}=0.3) were incubated with [^{3}H]-serine (3.3μCi/ml) for six hours. At hour three, cells were presented with 6748-481 (20μM), DMSO, or shifted to non-permissive temperature (37°C). Lipids were extracted and resolved by thin layer chromatography. PtdSer and PtdEtn species were harvested, quantified by liquid scintillation counting, and data expressed as precursor/product ratios. Values represent mean ± s.e.m from at least 3 independent experiments. Defects in Sfh4-dependent conversion of PtdSer to PtdEtn present high PtdSer/PtdEtn ratios – e.g. *psd1*Δ *sfh4*Δ control strains. Statistical comparisons of values used the ‘unpaired two-tailed t-test” relative to DMSO control, where # (P = 0.0495), ## (P = 0.002), ** (P = 0.0051), *** (P = 0.0004). Bar, 1 cm.

Author Manuscript Author Manuscript Author Manuscript Author Manuscript

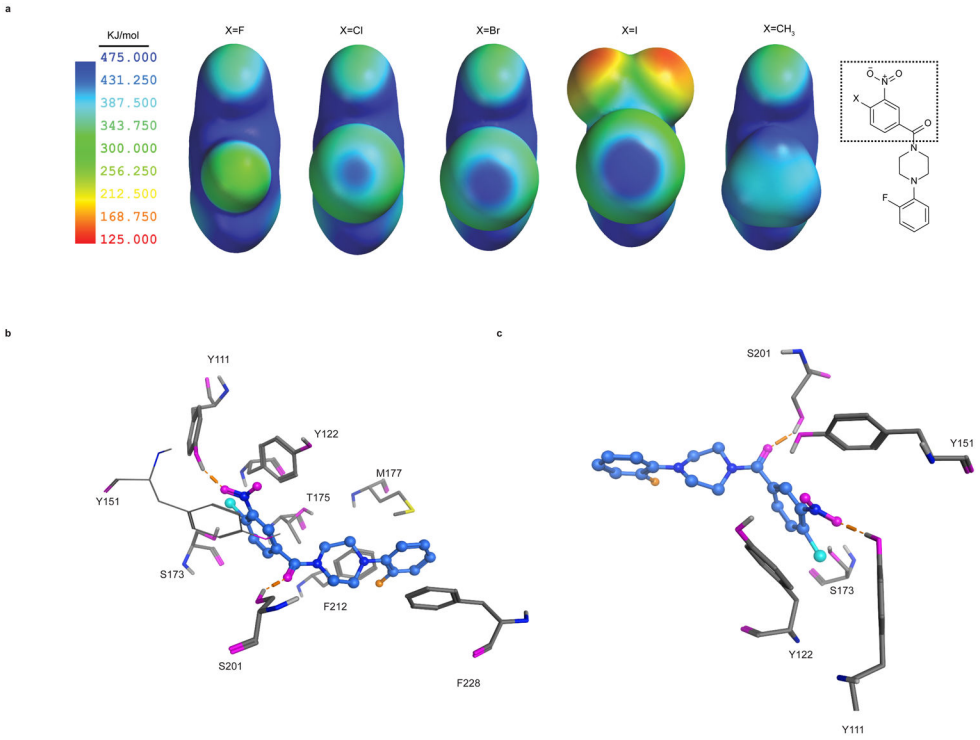

Figure 6. Model for NPPM-mediated inhibition of Sec14

(**a**) Simulations of the electrostatic potentials of the indicated NPPM activated aryl halides predict formation of progressively larger electropositive σ-holes in the -Cl, -Br and -I activated aryl halides, respectively. The -CH_3 and -F derivatives are forecast to be incapable of forming significant σ-holes. (**b**) NPPM binding mode 2 is most consistent with the various data and is depicted within the Sec14 hydrophobic pocket. H-bonds (orange), carbon (blue), oxygen (magenta), nitrogen (dark blue), chlorine (teal) and fluorine (orange). (**c**) A focused view of NPPM binding mode 2 highlighting Sec14 residues which form the PtdCho headgroup coordinating substructure, and whose alteration renders Sec14 resistant to NPPM inhibition. Hydrogen bonds (orange), carbon (blue), oxygen (red), nitrogen (dark blue), chlorine and fluorine (green).